Segregation by size difference in binary suspensions of fluid droplets in channel flow

doi: 10.3233/bir-130638

Biorheology 50 (2013) 149–163
DOI 10.3233/BIR-130638
IOS Press

Segregation by size difference in binary suspensions of fluid droplets in channel flow

Masato Makino and Masako Sugihara-Seki *
Faculty of Engineering Science, Kansai University, Osaka, Japan

Received 5 April 2013
Accepted in revised form 6 June 2013

Abstract. In channel flow of multicomponent suspensions, segregation behavior of suspended components perpendicular to the flow direction is often observed, which is considered to be caused by the differential properties of the lateral migration depending on their shape, size, flexibility, and other characteristics. In the present study, we investigate the effect of size differences between suspended components on the segregation behavior, by a two-dimensional numerical simulation for binary dispersed suspensions of fluid droplets of two different sizes subjected to a plane Poiseuille channel flow. The small and large droplets are assumed to have equal surface tensions and equal viscosity ratios of internal to external fluids. The time evolutions of the lateral positions of large and small droplets relative to the channel centerline were computed by changing the area fraction of the small droplets in a mixture with a constant total area fraction. The large droplets are found to migrate closer to the channel centerline and the small droplets are found to migrate closer to the channel wall compared to the corresponding lateral positions in mono-dispersed suspensions at the same area fractions, although the mean lateral positions of the large and small droplets in mono-dispersed suspension are comparable. This segregation behavior as well as the margination of small droplets are enhanced when the size difference between large and small droplets is increased and the area fraction of large droplets is increased. These results may arise from higher tendencies for the large droplets to approach the channel centerline compared to the small droplets, which consequently expel small droplets from the central region toward the channel walls.

Keywords: Droplets dispersion, margination

1. Introduction

In the flow of suspensions, the migration of suspended particles perpendicular to the flow direction is gaining considerable attention in a variety of fields [14], although numerous phenomena related to lateral migration have long been known in fluid mechanics. For example, rigid spheres suspended in a Poiseuille flow through circular tubes migrate toward a certain radial position apart from the centerline at finite Reynolds numbers, which is referred to as the tubular pinch effect or the Segré–Silberberg effect [20]. In contrast, deformable particles in tube flows migrate toward the tube centerline at low and moderate Reynolds numbers [9,10]. Chiral particles subjected to shear flows move parallel to the vorticity vector, i.e., perpendicular to the main flow, and their direction of motion could be opposite, depending on the particle's handedness [16].

Due to the different migration properties of suspended particles, multicomponent suspensions often display segregation behaviors in channel flow in such a way that one component approaches the centerline of the channel, whereas another component migrates toward the walls of the channel. One prominent

*Address for correspondence: Dr. Masako Sugihara-Seki, Department of Pure and Applied Physics, Kansai University, 3-3-35 Yamate-cho, Suita, Osaka 564-8680, Japan. Tel.: +81 6 6368 0866; E-mail: sekim@kansai-u.ac.jp.

example is blood flow through microvessels or microchannels. Blood is primarily a suspension of red cells with a small number of white cells and platelets. Normal red cells are highly deformable, and so tend to approach the vessel centerline, and a red-cell-depleted layer, referred to as the cell-free layer, is formed along the periphery of vessels. On the other hand, platelets, which are much smaller and less deformable compared to red cells, are displaced from the vessel centerline and are plentiful in the vicinity of the vessel wall [1,5,19,22,23,25,26]. This phenomenon is commonly referred to as margination, or near-wall excess (NWE). White blood cells, which are larger and much less deformable compared to red cells, are also known to marginate near the vessel wall in venules, especially under low-flow conditions [7,11,17,18]. The margination of platelets and white cells in blood flow is evidently expedient in hemostatic and immune functions, respectively, at physiological and pathological states. Recently, microfluidic devices have been developed to separate blood components based on differences in their migration properties [21].

Several previous simulation studies, as well as model studies, have investigated the lateral migration and segregation behaviors of multicomponent suspensions [4,6,8,28]. Despite the importance of segregation phenomena, its mechanism has not yet been fully elucidated. Direct fluid mechanical simulations of mixed suspensions containing floppy and stiff particles have recently demonstrated that the membrane rigidity of suspended particles play a crucial role in their segregation behavior in confined flows [12,13,15].

In the present study, we focus on the effect of the size difference in suspended particles and simulate their lateral migration behaviors using suspensions of two-dimensional fluid droplets of two different sizes in a channel flow. The surface tension and viscosity ratio of the internal to external fluids are assumed to be the same for large and small droplets. The motion and deformation of droplets immersed in a plane Poiseuille flow through a two-dimensional channel are computed using a front-tracking method [24]. The breakup and coagulation of the droplets are not considered in the current study.

The front-tracking method is an efficient numerical scheme for analyzing the dynamics of multiphase flows, containing droplets, capsules, or blood cell models. The circumference of suspended particles is expressed using Lagrangian meshes, which are superimposed on an Eulerian mesh for the Navier–Stokes equations' solver. The nodes on the Lagrangian mesh are advected with a velocity that is determined by interpolation of the velocities on neighboring Eulerian nodes.

The remainder of the present paper is organized as follows. In Section 2, the proposed simulation method using a two-dimensional front-tracking method is introduced, and the numerical accuracy of the developed simulator is assessed. In Section 3, the formulation and simulation procedure is presented. In Section 4, the results of the simulation for binary dispersed suspensions of fluid droplets, as well as mono-dispersed suspensions, are presented. Finally, a summary is presented in Section 5.

2. Simulation method

We consider the flow of suspensions of droplets, the viscosity of which is η and the mass density of which is ρ. The droplets are suspended in a Newtonian fluid having viscosity η_s and density ρ_s. The velocity $\mathbf{v}(\mathbf{r})$ and the pressure $p(\mathbf{r})$ of the fluids in the presence of a volume force $\mathbf{f}$ are governed by the Navier–Stokes equations:

$$\rho_\alpha\left(\frac{\partial \mathbf{v}}{\partial t} + \mathbf{v}\cdot\nabla\mathbf{v}\right) = -\nabla p + \nabla\cdot\eta_\alpha\big(\nabla\mathbf{v} + (\nabla\mathbf{v})^t\big) + \mathbf{f}, \tag{1}$$

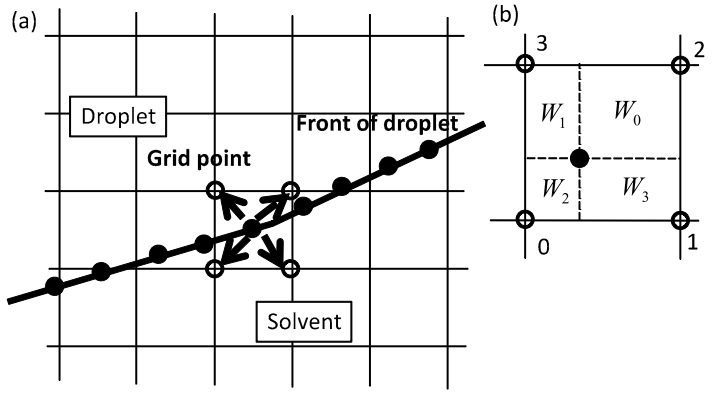

Fig. 1. Front of a droplet. (a) The information of the traction force and the velocity is exchanged between the droplet nodes and the fluid nodes by an interpolation using area weight functions. (b) The weight of the ith nodal value is the area fraction W_i ($i = 0, 1, 2, 3$).

and the continuity equation,

$$\nabla \cdot \mathbf{v} = 0, \tag{2}$$

where $\rho_\alpha = \rho_s$ or ρ, and $\eta_\alpha = \eta_\mathrm{s}$ or η for the external or internal fluid of the droplet. In the absence of external forces, the volume force results from the surface tension of the droplets, σ, which is given by

$$\mathbf{f} = \sigma\kappa\mathbf{n}\delta(\mathbf{r}), \tag{3}$$

where κ is the curvature of the interface, $\mathbf{n}$ is unit normal on the interface, and $\delta(\mathbf{r})$ is a delta function, which is equal to zero except at droplet interfaces. We solve these equations to obtain $\mathbf{v}(\mathbf{r})$ and $p(\mathbf{r})$ using an implicit fractional step method [24].

For analyzing the dynamics of droplets, we adopt a front-tracking method [24]. The front or the interface of a droplet is represented by connected marker points that are moved by the fluid (Lagrangian mesh). As shown in Fig. 1, this Lagrangian mesh is immersed in a regular grid used for solving the fluid motion (Eulerian mesh). We refer to the marker points on the interface as droplet nodes and refer to the grid points as fluid nodes.

Exchange of information, such as the force and the velocity, between the droplet nodes and the fluid nodes is necessary. The traction $\mathbf{f}(\mathbf{r}_d)$ at a droplet node, where $\mathbf{r}_d$ is the position of the node, is distributed to neighboring fluid nodes $\mathbf{r}_l$ in such a way that:

$$\mathbf{f}(\mathbf{r}_l) = \sum W(\mathbf{r}_l - \mathbf{r}_d)\mathbf{f}(\mathbf{r}_d)\frac{\Delta S}{\Delta x \Delta y}, \tag{4}$$

where the summation is made over the droplet nodes, $W(\mathbf{r})$ is a weight function, ΔS is the averaged length between node l and adjacent nodes, and Δx and Δy are the grid spacings of the Eulerian mesh. In the current study, the traction is assigned to four nearest fluid nodes and the weight function is given by

$$W(\mathbf{r}) = d\left(\frac{r_x}{\Delta x}\right) d\left(\frac{r_y}{\Delta y}\right), \tag{5}$$

where r_x and r_y are the x- and y-components of $\mathbf{r}$.

$$d(r) = \begin{cases} 1 - r, & 0 < r < 1, \\ 1 + r, & -1 < r < 0, \\ 0, & |r| \geqslant 1. \end{cases} \tag{6}$$

Here, Eqs (5) and (6) indicate that the weight function in Eq. (4) corresponds to the area fraction, as shown in Fig. 1(b). Although smoother distribution functions than the area weight functions are sometimes recommended, the area weight function worked well in the present study. Thus, we used this weight function, which is easy to implement.

In a similar manner, the velocity on the droplet node is evaluated by a weighted summation of the velocities on neighboring fluid nodes:

$$\mathbf{v}(\mathbf{r}_d) = \sum W(\mathbf{r}_d - \mathbf{r}_l)\mathbf{v}(\mathbf{r}_l). \tag{7}$$

When the velocities on the droplet nodes at time step n are obtained, their new positions at the next time step are given based on the first-order Euler method by:

$$\mathbf{r}_d^{n+1} = \mathbf{r}_d^n + \mathbf{v}^n(\mathbf{r}_d)\Delta t, \tag{8}$$

where Δt is time increment in a step. However, this simple update method sometimes leads to a drastic change in distance between adjacent nodes, which makes the time marching of the advection of the droplet nodes unstable. In order to avoid this instability, we adopt an algorithm in which the droplet nodes are moved in the tangential direction along the droplet interface, according to Ref. [30].

As the droplet interface advects, the viscosity and density near the interface must be updated. Rather than the method using a Poisson equation proposed by Tryggavson et al. [24], we herein adopt an approach by Zhang et al. [27] in terms of a smoothed Heaviside function for reducing the computational time.

There are several numerical schemes to avoid overlapping of neighboring droplets. In the present study, we introduce a buffer-zone around each droplet to track the distance between droplets that are identified as undergoing collision, in a way similar to Almomani et al. [2]. We set the thickness of the buffer-zone to equal the grid spacing, within which neighboring droplet surfaces cannot approach each other by forcing the vertex on the surface to move in the direction normal to the droplet surface. This algorithm is also used to avoid overlapping between a droplet and the channel wall.

In order to assess the accuracy of our simulator, we have applied the present numerical method to a single droplet immersed in a Couette flow between two-parallel plates and compared the obtained results with previous studies. For a droplet of the viscosity ratio $\eta/\eta_s = 1$ and the size ratio $L_y/a = 8$, where a is the droplet radius at rest and L_y is the distance between the two plates, we computed the time evolution of the droplet shape in the Couette flow, starting from an undeformed circular shape and, in Fig. 2, plotted the deformation parameter D and the orientation angle θ relative to the undisturbed flow for stationary shapes as a function of the capillary number $Ca = 2\eta_s u_0 a/\sigma L_y$. Here, u_0 is the velocity of the plates, and $D = (L - M)/(L + M)$, where L and M are the major and minor axes of an ellipse approximating the droplet shape. A comparison of this figure with Fig. 2(c) in Zhou and Pozrikidis [29], which treated the same problem using the boundary integral method, exhibited close agreement. In particular, for small *Ca*, at which we consider the flow of suspensions in the following sections, the agreement was excellent.

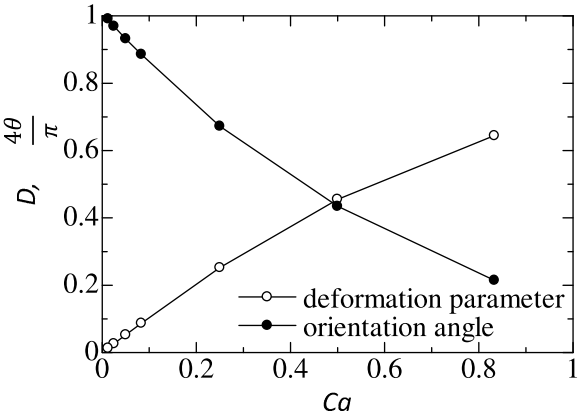

Fig. 2. The deformation parameter and the orientation angle for droplets of $\eta/\eta_s = 1$ and $L_y/a = 8$ in a Couette flow as a function of the capillary number *Ca*.

3. Problem statement

We consider binary dispersed suspensions of large and small droplets immersed in a plane Poiseuille flow in a two-dimensional channel, as shown in Fig. 3. The distance between the two channel walls is expressed as L_y, and the computational domain has length L_x in the flow direction. The radius of the large droplets at rest is denoted as a_0, which will be taken as the unit of length throughout the present study, and we herein treat the cases of $L_x/a_0 = 16$ and $L_y/a_0 = 9.6$.

Poiseuille flow is induced by applying a pressure difference, Δp, across upstream and downstream sections of the channel, where we apply a periodic boundary condition. No-slip boundary conditions, i.e., $\mathbf{v} = 0$, are imposed on the surfaces of the channel walls. As an initial condition for the velocity field, we assume a Poiseuille flow, the maximum velocity of which is given by $u_{\max} = (\Delta p L_y^2)/(8\eta_s L_x)$ in the absence of droplets.

We express the radius of small droplets at rest as a_1 and the numbers of the large and small droplets in the computational domain as N_0 and N_1, respectively. It is assumed that the large and small droplets have the same surface tension σ and the same viscosity η.

The area fractions of the large and small droplets, ϕ_0 and ϕ_1, and the area fraction of the mixture, ϕ, are defined by

$$\phi_0 = \frac{N_0 \pi a_0^2}{L_x \cdot L_y}, \qquad \phi_1 = \frac{N_1 \pi a_1^2}{L_x \cdot L_y} \tag{9}$$

and

$$\phi = \phi_0 + \phi_1. \tag{10}$$

The ratio of the small droplets in the mixture, ψ, is given by

$$\psi = \phi_1/\phi. \tag{11}$$

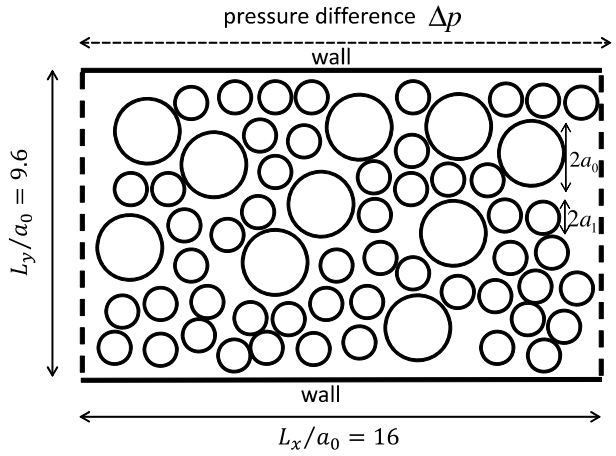

Fig. 3. Configuration for binary dispersed suspensions of large and small droplets. The large droplets have radius a_0 at rest, and the small droplets have radius a_1 at rest. We consider a pressure-driven flow in a two-dimensional channel of width L_y, induced by applying a pressure difference Δp across a distance L_x in the flow direction.

We are interested in the lateral positions of the droplets. Thus, we define the mean lateral position of the droplet α relative to the channel centerline as

$$\langle y_\alpha \rangle = \sqrt{\frac{1}{N_\alpha} \sum_{i=0}^{N_\alpha - 1} \left(y_{\alpha,i} - \frac{L_y}{2} \right)}, \quad \alpha = 0, 1, \tag{12}$$

where $y_{\alpha,i}$ represents the distance of the center of the ith droplet of α kind from the lower wall of the channel. In the present simulation, we examine $\langle y_0 \rangle$ and $\langle y_1 \rangle$ as a function of time.

There are four important non-dimensional parameters: the Reynolds number $Re = \rho_s a_0 u_{\max}/\eta_s$, the capillary number $Ca = \eta_s a_0 u_{\max}/\sigma L_y$, the viscosity ratio η/η_s and the density ratio ρ/ρ_s. As a first step to study the size segregation of droplets, we start with a case in which the inertial effect is not important and the deformation of the droplets is not large. For that purpose, the present study is confined to the case of $Re = 0.72$, $Ca = 0.075$, $\eta/\eta_s = 1$ and $\rho/\rho_s = 1$. More general cases will be considered in our subsequent studies. In the present work, we focus on the effects of the size difference a_1/a_0 and the fractional ratio ψ on the segregation behavior.

The initial configurations of the droplets are chosen according to the results of a molecular dynamics simulator for rigid beads, COGNAC [3] of OCTA, which can be accessed at http://octa.jp. The COGNAC simulation can determine the positions of rigid beads of radius a_0 or a_1, the interaction energy of which reaches the minimum under a truncated Lennard–Jones potential and a Lennard–Jones wall. In the present study, we examine cases involving various values of a_1, ϕ_0, ϕ_1 and ψ. For each case, we performed such COGNAC simulations five times to obtain five sets of initial configurations of droplets for the present study. In the next section, we report the ensemble averaged values of the results over five runs starting from these configurations.

4. Results and discussion

4.1. Mono-dispersed suspensions

Before examining binary dispersed suspensions, we first simulate the behaviors of mono-dispersed suspensions of large or small droplets as a reference state. We consider the cases of the droplet radius at rest, with a being a_0, $a_0/\sqrt{2}$, $a_0/\sqrt{3}$ or $a_0/2$.

As examples of initial configurations for mono-dispersed suspensions, Fig. 4(a) and (c) are snapshots at non-dimensional time $tu_{\max}/a_0 = 0$ for the droplet radii of a_0 and $a_0/2$, respectively, for an area fraction of $\phi = 0.511$. Starting from these initial configurations, we obtained the configurations shown in Fig. 4(b) and (d), respectively, at $tu_{\max}/a_0 = 2{,}778$, which is the final computation time.

Figure 4(a) shows four rows of droplets aligned along the flow direction. These rows of droplets are also shown in Fig. 4(b). These rows are found to be quite stable over the computational time. Comparison of Fig. 4(a) and (b) reveals that the rows next to the lower and upper channel walls move closer to the channel walls, and the droplets in these rows deform more than the droplets in the other rows due to the larger velocity gradients in the vicinity of the channel walls. On the other hand, for small droplets of radius $a_0/2$, as shown in Fig. 4(d), small droplets seldom form long, stable rows, and their lateral positions are changed stochastically as a result of fluid dynamic interactions with neighboring droplets, despite having the same area fraction, i.e., $\phi = 0.511$, as shown in Fig. 4.

Figure 5(a) and (b) shows final snapshots of mono-dispersed suspensions at $tu_{\max}/a_0 = 2{,}778$ for the droplet radius a_0 and $a_0/2$, respectively. Figure 5(a) shows that, at a low area fraction of $\phi = 0.102$, large droplets of radius a_0 are almost aligned in two rows parallel to the flow direction. Moreover, these droplets form three rows at $\phi = 0.205$ and four rows at $\phi = 0.409$. On the other hand, Fig. 5(b) shows that small droplets of radius $a_0/2$ are distributed almost randomly in the channel and are occasionally aligned parallel to the flow direction, except next to the channel walls.

Figure 6(a) and (b) shows the time evolutions of the mean lateral positions of droplets for radii of $a = a_0$ and $a_0/2$, respectively. In the case of low area fractions, such as $\phi = 0.102$ and $\phi = 0.205$, the mean lateral positions of both types of droplets decrease with time, indicating that the droplets migrate

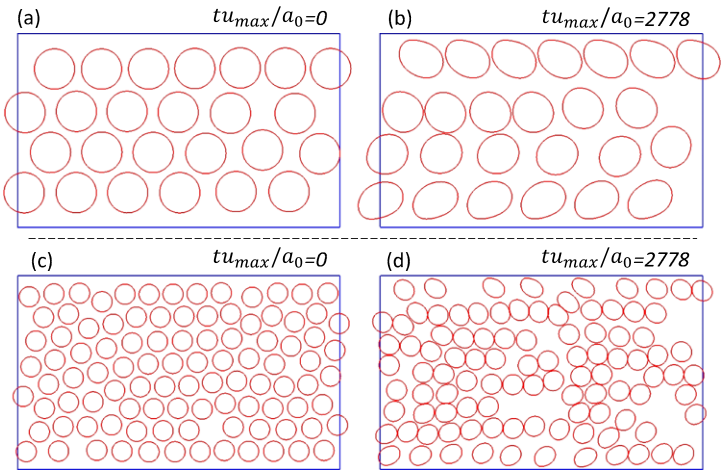

Fig. 4. Snapshots of mono-dispersed suspensions of droplets of radius a with area fraction $\phi = 0.511$. (a) $a = a_0$, $tu_{\max}/a_0 = 0$, (b) $a = a_0$, $tu_{\max}/a_0 = 2{,}778$, (c) $a = a_0/2$, $tu_{\max}/a_0 = 0$ and (d) $a = a_0/2$, $tu_{\max}/a_0 = 2{,}778$. (Colors are visible in the online version of the article; http://dx.doi.org/10.3233/BIR-130638.)

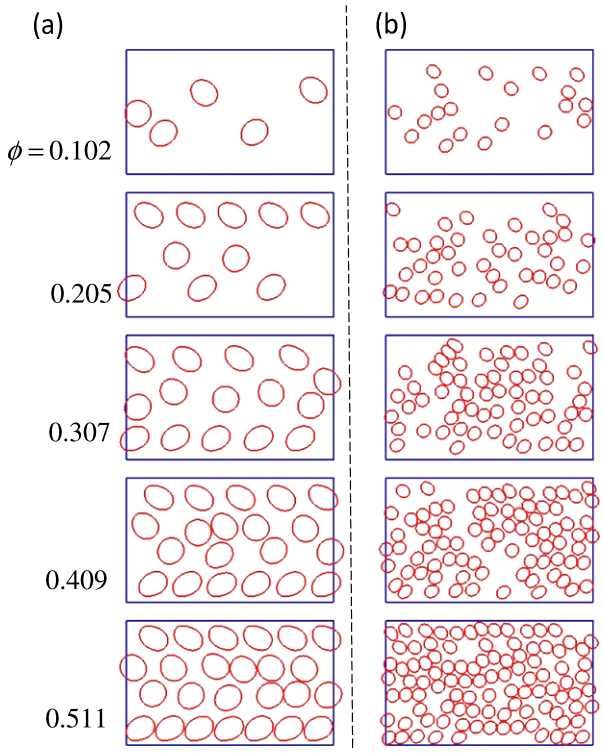

Fig. 5. Snapshots of mono-dispersed suspensions of droplets for various area fractions ϕ: (a) $a = a_0$ and (b) $a = a_0/2$. From top to bottom, the images show the cases for $\phi = 0.102$, 0.205, 0.307, 0.409 and 0.511. (Colors are visible in the online version of the article; http://dx.doi.org/10.3233/BIR-130638.)

toward the channel centerline with time. In particular, at $\phi = 0.102$, the final mean lateral positions at $tu_{\max}/a_0 = 2{,}778$ are much closer to the channel centerline compared to the initial positions. This result may be well understood from the fact that isolated liquid drops or deformable particles immersed in channel flow approach the channel centerline at low Reynolds numbers [9,10]. In contrast, at higher area fractions, Fig. 6 shows that the mean lateral positions of the large droplets increase with time, which is evidently due to mutual interactions of the droplets, whereas the mean lateral positions of the small droplets are almost constant. The final mean lateral positions are found to increase with increasing area fraction ϕ for both types of droplets. This behavior is summarized in Fig. 7, including the behaviors for other droplet radii.

Figure 7 shows the mean lateral positions averaged over the last 1,000 units of non-dimensional time as a function of the area fraction for radii of a_0, $a_0/\sqrt{2}$, $a_0/\sqrt{3}$ and $a_0/2$. The terminal mean lateral positions obtained in this manner vary similarly with ϕ for all types of droplets. In particular, the three lines for $a = a_0/\sqrt{2}$, $a_0/\sqrt{3}$ and $a_0/2$ in Fig. 7 are almost indistinguishable.

4.2. Binary dispersed suspensions

Next, we consider the lateral migration of binary dispersed suspensions of large and small droplets. The large droplets have a radius of a_0 at rest, and the small droplets have a radius of a_1 at rest. In this subsection, we report the results for varying the ratio ψ while the total area fraction ϕ is kept constant.

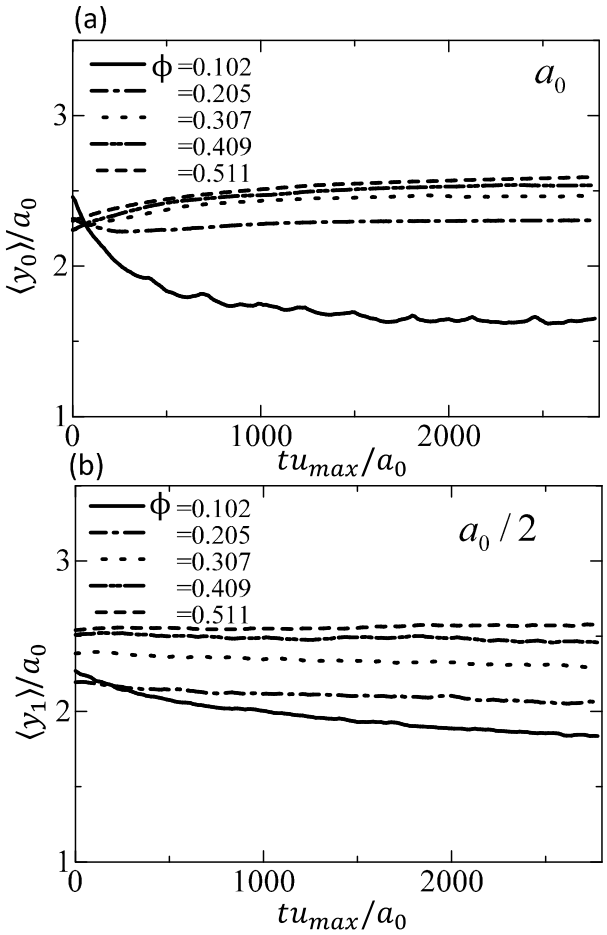

Fig. 6. Time evolutions of the mean lateral positions of mono-dispersed suspensions for $\phi = 0.102$, 0.205, 0.307, 0.409 and 0.511: (a) $a = a_0$ and (b) $a = a_0/2$.

Several examples of snapshots at the final computational time are shown in Fig. 8. Figure 8(a)–(c) represents the cases of $a_1 = a_0/\sqrt{2}$, $a_0/\sqrt{3}$ or $a_0/2$, respectively, at $\psi = 0.4$ and $\phi = 0.511$, corresponding to the cases of $\phi_0 = 0.307$ and $\phi_1 = 0.205$. In Fig. 8(a), large and small droplets of comparable sizes are distributed randomly in the mixture in the channel, whereas in Fig. 8(c), the arrangement of the large droplets in the presence of much smaller droplets appears similar to that of mono-dispersed suspensions of the large droplets shown in Fig. 5(a) at the same area fraction of $\phi_0 \approx 0.3$. Figure 8(d) shows a snapshot for $a_1 = a_0/2$ at $\psi = 0.8$ and $\phi = 0.511$ which corresponds to the case of $\phi_0 = 0.102$ and $\phi_1 = 0.408$. Comparison of this figure with Fig. 5(a) at $\phi_0 \approx 0.1$ reveals a similarity in the arrangement of the large droplets. Together with the similarity between Figs 8(c) and 5(a) at $\phi_0 \approx 0.3$ mentioned above, this result indicates that the presence of the small droplets of radius $a_1 = a_0/2$ has a slight effect on the large droplet configuration itself, although a line of small droplets is often formed next to the channel wall in binary dispersed suspensions (Fig. 8(c) and (d)). This line formation of the small droplets is expected to decrease the mean lateral position of the large droplets and to increase the mean lateral position of the small droplets.

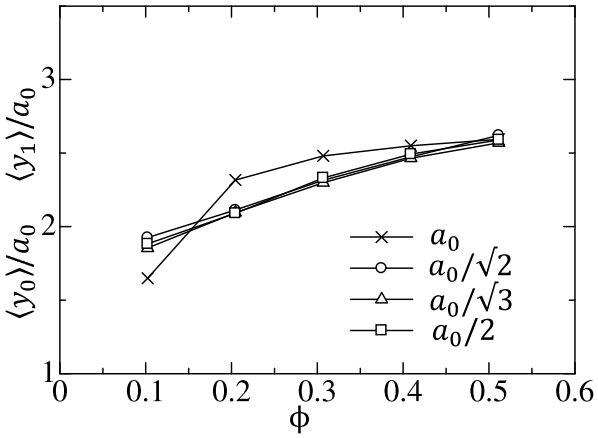

Fig. 7. Mean lateral positions of mono-dispersed suspensions averaged over the last 1,000 units of non-dimensional time for $a = a_0$ (cross symbols), $a_0/\sqrt{2}$ (circles), $a_0/\sqrt{3}$ (triangles) and $a_0/2$ (squares) as a function of the area fraction ϕ. y_0 and y_1 represent the distance of large and small droplet centers from the channel centerline, respectively.

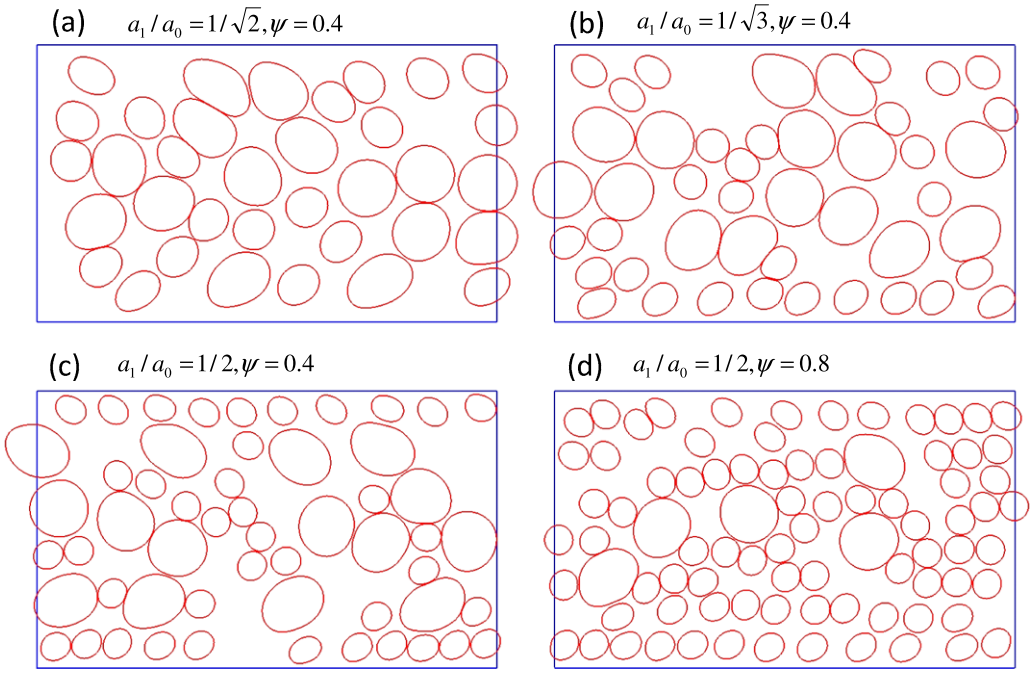

Fig. 8. Snapshots of binary dispersed suspensions of large and small droplets for $\phi = 0.511$ at $tu_{\max}/a_0 = 2{,}778$: (a) $a_1 = a_0/\sqrt{2}$, $\psi = 0.4$, (b) $a_1 = a_0/\sqrt{3}$, $\psi = 0.4$, (c) $a_1 = a_0/2$, $\psi = 0.4$ and (d) $a_1 = a_0/2$, $\psi = 0.8$. (Colors are visible in the online version of the article; http://dx.doi.org/10.3233/BIR-130638.)

Figure 8(c) and (d) shows that the small droplets of radius $a_1 = a_0/2$ are distributed in the spaces among the large droplets. In other words, the small droplets are expelled from the central region toward the channel wall by the large droplets, due to higher tendencies for the large droplets to approach the channel centerline compared to the small droplets. Thus, the mean lateral positions of the small droplets are expected to be larger, whereas the mean lateral positions of the large droplets are expected to be

smaller than the corresponding values of mono-dispersed suspensions at the same area fractions. These features can be confirmed below in Fig. 11.

The simulations of the present study indicate that the line of small droplets formed adjacent to the lower wall in Fig. 8(b) sometimes breaks and becomes shorter or longer with time, whereas the line remains longer in Fig. 8(c) and (d). This trend indicates that the lines of small droplets are more stable when the size difference between large and small droplets is larger.

Figures 9 and 10 show the time evolutions of the mean lateral positions of large and small droplets for radii of the small droplets of $a_1 = a_0/\sqrt{2}$ and $a_0/2$, respectively. Figure 9 shows that the mean lateral positions of small droplets for $a_1 = a_0/\sqrt{2}$ are approximately constant with time for various values of ψ and that their final values are approximately the same, irrespective of ψ, although the final positions of the large droplets decrease slightly with ψ. In contrast, for the case of $a_1 = a_0/2$ shown in Fig. 10 the mean lateral positions of small droplets increased considerably, and those of large droplets decreased significantly with time, except for the case of $\psi = 0$, i.e., in the absence of small droplets (mono-dispersion). These results for $a_1 = a_0/2$ indicate that the small droplets are displaced further

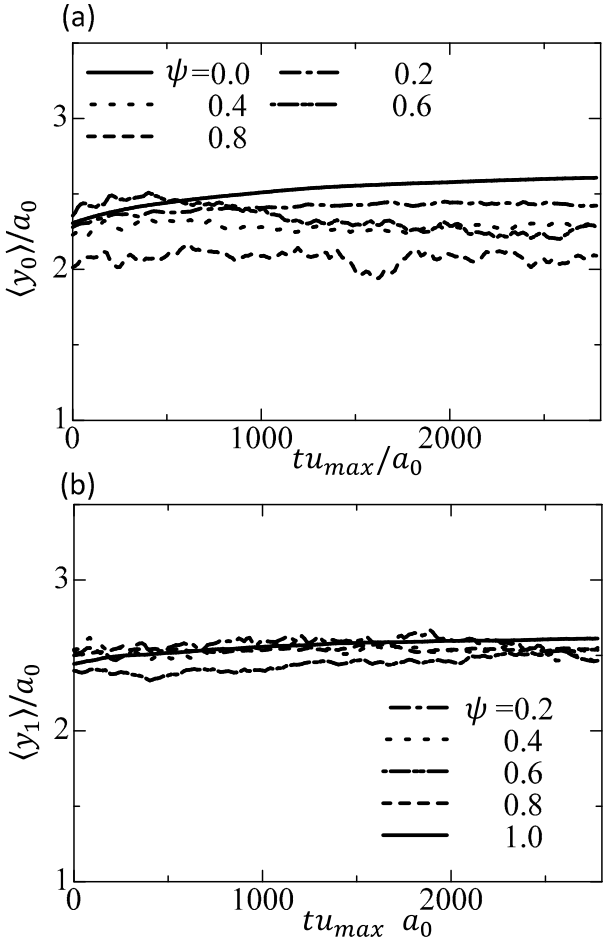

Fig. 9. Time evolutions of the mean lateral positions of binary dispersed suspensions for $a_1 = a_0/\sqrt{2}$, at $\phi = 0.511$ and $\psi = 0$, 0.2, 0.4, 0.6, 0.8 and 1.0. (a) Mean lateral positions of large droplets $\langle y_0 \rangle / a_0$, (b) mean lateral positions of small droplets $\langle y_1 \rangle / a_0$.

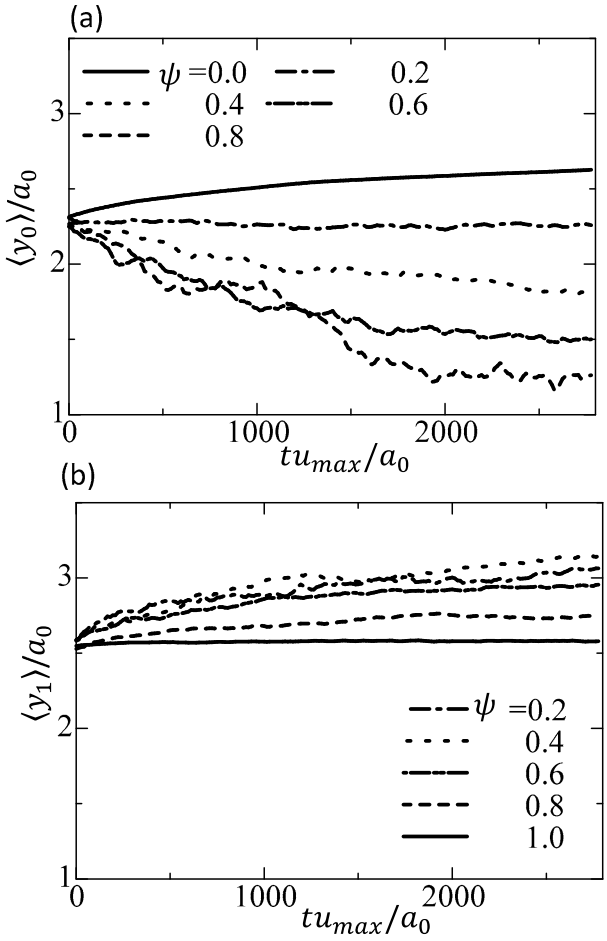

Fig. 10. Time evolutions of the mean lateral positions of binary dispersed suspensions for $a_1 = a_0/2$ at $\phi = 0.511$ and $\psi = 0$, 0.2, 0.4, 0.6, 0.8 and 1.0. (a) Mean lateral positions of large droplets $\langle y_0 \rangle / a_0$, (b) mean lateral positions of small droplets $\langle y_1 \rangle / a_0$.

from the channel centerline or migrate toward the channel walls with time and that the large droplets in the mixture move toward the channel centerline. These behaviors correspond to the segregation of binary dispersed suspensions, as shown more clearly in Fig. 11.

The variations of the terminal mean lateral positions of large and small droplets are shown in Fig. 11 as a function of ψ, for $a_1 = a_0/\sqrt{2}$, $a_0/\sqrt{3}$ and $a_0/2$ at $\phi = 0.511$. For reference, the averaged lateral positions in the mixture are calculated by:

$$\langle y \rangle = (1 - \psi)\langle y_0 \rangle + \psi \langle y_1 \rangle. \tag{13}$$

The values of $\langle y \rangle / a_0$ are also plotted by dashed lines for $a_1 = a_0/\sqrt{2}$, $a_0/\sqrt{3}$ and $a_0/2$ in Fig. 11. These three lines approximately coincide with each other, being nearly constant but slightly concave curves as a function of ψ. This concavity suggests that the mixture of large and small droplets may decrease their averaged mean lateral positions compared to the mono-dispersion for a constant ϕ.

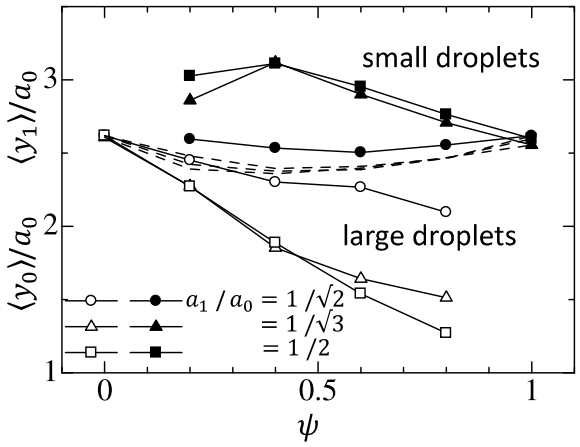

Fig. 11. Mean lateral positions of large droplets (open symbols) and small droplets (closed symbols) averaged over the last 1,000 units of non-dimensional time at $\phi = 0.511$ for $a_0/\sqrt{2}$ (circles), $a_0/\sqrt{3}$ (triangles) and $a_0/2$ (squares). Dashed lines represent the averaged lateral positions in the mixture $\langle y\rangle/a_0$.

In Fig. 11, comparison of closed symbols for small droplets and the corresponding open symbols for large droplets reveals that the mean lateral positions of the small droplets are always larger than those of the large droplets, indicating the segregation of droplets induced by the size difference. For $a_1 = a_0/\sqrt{3}$ and $a_0/2$, the difference between $\langle y_1\rangle/a_0$ and $\langle y_0\rangle/a_0$ is significant and is greater than unity (the difference between $\langle y_1\rangle$ and $\langle y_0\rangle$ is larger than a_0) for ψ larger than 0.4, whereas the difference is small for $a_1 = a_0/\sqrt{2}$. These results suggest that a certain difference between large and small droplet sizes is necessary in order to generate substantial segregations of droplets.

The variations of $\langle y_0\rangle$ and $\langle y_1\rangle$ with ψ in Fig. 11 indicate that, with an increasing fraction of small droplets, the large droplets become displaced toward the channel centerline, whereas, with an increasing fraction of large droplets, the small droplets become displaced toward the channel wall. These trends are parallel to the segregation behavior of stiff and floppy particles reported in Kumar and Graham [13], which numerically treated the binary suspension of stiff and floppy particles subjected to a plane channel flow. They reported that stiff particles are increasingly displaced toward the channel walls with an increasing fraction of floppy particles, whereas the floppy particles increasingly accumulate near the channel centerline with increasing fraction of stiff particles (see Fig. 4 in [13]). Thus, the behaviors of the large and small droplets in the present study are similar to those of the floppy and stiff particles, respectively. They demonstrated through a model study of heterogeneous pair collisions involving stiff and floppy particles that, compared to the floppy particle, the stiff particle experiences a larger cross-stream displacement as a result of the collision and explained the segregation of the floppy and stiff particles in the mixture by applying this result to floppy and stiff particles placed in the near-wall region. Our preliminary study of collisions of droplets suspended in Couette flow showed that, as a result of pair collisions of a large and a small droplet, the lateral displacement of the small droplet is larger than that of the large droplet, which is in accord with Ref. [13] if the small droplet is replaced by the stiff particle and the large droplet is replaced by the floppy particle. Accordingly, a similar discussion to that of Kumar and Graham [13] may be applied to explain the segregation behavior shown in Fig. 11.

Note that, in Fig. 11, the terminal mean lateral positions of the small droplets attain the maximum, i.e., the margination of the small droplets is the most enlarged, at $\psi = 0.4$. There may be a value of ψ at which the margination is most efficiently induced by the size difference.

So far, the cases for the total area fraction $\phi = 0.511$ have been reported. For $\phi \approx 0.2$, 0.3 and 0.4, we have obtained similar plots to Fig. 11. It is found that the variations of $\langle y_0 \rangle$ and $\langle y_1 \rangle$ with ψ are qualitatively similar for all cases we have examined.

In the present study, we have investigated the difference in size of suspended droplets while maintaining the surface tension and the viscosity ratio of the internal and external fluids constant. The surface tension and the viscosity ratio affect the extent of deformation of the droplets as well as the migration velocity subjected to shear. The effects of these factors on segregation and margination will be reported in a future study. Additionally, in order to elucidate the mechanism of the segregation behavior presented here and to reveal the scaling behavior of binary dispersed suspensions of droplets, we are now refining our simulation system to cover wider range of capillary numbers and other parameter values.

We briefly mention the advantages and limitations of using two-dimensional simulations. The dynamics of suspension of flexible particles are complex and a number of phenomena are not well understood. A two-dimensional approach allows exploration of effects that can occur in a system with fewer degrees of freedom, allowing more systematic exploration of parameter space and facilitating interpretation of the results. On the other hand, there may be other significant effects that come into play in three dimensions. The findings and predictions from two-dimensional models should ultimately be tested using three-dimensional simulations and experimentally.

5. Summary

The motion and deformation of mono-dispersed and binary dispersed suspensions of droplets subjected to a pressure-driven flow in a two-dimensional channel are calculated by a front-tracking method. In the mono-dispersed suspensions, the terminal mean lateral positions of the droplets increase in a similar manner with increasing area fraction for all of the droplet radii considered herein. In binary dispersed suspensions of large and small droplets, the configurations of the large droplets are only weakly affected by the presence of the small droplets if there is a certain difference in size between large and small droplets. The small droplets are distributed in the spaces among the large droplets and often form a line along the channel wall. As a result, the mean lateral positions of the large droplets become closer to the channel centerline and those of the small droplets become closer to the channel wall, as compared to the mono-dispersed suspension. This segregation, as well as the margination of small droplets, is enhanced as the size difference of the droplets and the area fraction of large droplets increase.

Acknowledgements

The present study was supported by JSPS KAKENHI Grant Numbers 23360087, 25800238, 25630057, the Special Research Fund of Kansai University and a Kansai University Grant-in-Aid for Progress in Graduate Research. The authors are deeply indebted to the Research Center for Advanced Computing Infrastructure of the Japan Advanced Institute of Science and Technology (JAIST) for providing resources used in the present study. GOURMET of the OCTA integrated simulation system (http://octa.jp) was used for data management and visualization.

References

[1] P.A. Aarts, S.A. van den Broek, G.W. Prins, G.D. Kuiken, J.J. Sixma and R.M. Heethaar, Blood platelets are concentrated near the wall and red blood cells in the center in flowing blood, *Arterioscler. Thromb. Vasc. Biol.* **8** (1988), 819–824.

[2] T. AlMomani, H.S. Udaykumar, J.S. Marshall and K.B. Chandran, Micro-scale dynamic simulation of erythrocyte-platelet interaction in blood flow, *Ann. Biomed. Eng*. **36** (2008), 905–920.
[3] T. Aoyagi, F. Sawa, T. Shoji, H. Fukunaga, J. Takimoto and M. Doi, A general-purpose coarse-grained molecular dynamics program, *Comput. Phys. Commun*. **145** (2002), 267–279.
[4] L. Crowl and A.L. Fogelson, Analysis of mechanisms for platelet near-wall excess under arterial blood flow conditions, *J. Fluid. Mech*. **676** (2011), 348–375.
[5] E.C. Eckstein, A.W. Tilles and F.J. Millero, Conditions for the occurrence of large near wall excesses of small particles during blood flow, *Microvasc. Res.* **36** (1988), 31–39.
[6] D.A. Fedosov, J. Fornleitner and G. Gompper, Margination of white blood cells in microcapillary flow, *Phys. Rev. Lett*. **108** (2012), 028104.
[7] J.C. Firrel and H.H. Lipowsky, Leukocyte margination and deformation in mesenteric venules of rat, *Am. J. Physiol. Heart Circ. Physiol*. **256** (1989), H1667–H1674.
[8] J.B. Freund, Leukocyte margination in a model microvessel, *Phys. Fluids* **19** (2007), 023301.
[9] H.L. Goldsmith and S.G. Mason, The flow of suspensions through tubes. I. Single spheres, rods and discs, *J. Colloid Int. Sci*. **17** (1962), 448–476.
[10] H.L. Goldsmith and S.G. Mason, The microrheology of dispersions, in: *Rheology: Theory and Applications*, F.R. Eirich, ed, Vol. 4, Academic Press, New York, 1967.
[11] H.L. Goldsmith and S. Spain, Margination of leukocytes in blood flow through small tubes, *Microvasc. Res*. **27** (1984), 204–222.
[12] C.W. Hsu and Y L. Chen, Migration and fractionation of deformable particles in microchannel, *J. Chem. Phys*. **133** (2010), 034906.
[13] A. Kumar and M.D. Graham, Segregation by membrane rigidity in flowing binary suspensions of elastic capsules, *Phys. Rev. E* **84** (2011), 066316.
[14] A. Kumar and M.D. Graham, Margination and segregation in confined flows of blood and other multicomponent suspensions, *Soft. Matter.* **8** (2012), 10536–10548.
[15] A. Kumar and M.D. Graham, Mechanism of margination in confined flows of blood and other multicomponent suspensions, *Phys. Rev. Lett*. **109** (2012), 108102.
[16] M. Makino and M. Doi, Migration of twisted ribbon-like particles in simple shear flow, *Phys. Fluids* **17** (2005), 103605.
[17] R.J. Melder, J. Yuan, L.L. Munn and R.K. Jain, Erythrocytes enhance lymphocyte rolling and arrest *in vivo*, *Microvasc. Res*. **59** (2000), 316–322.
[18] M.J. Pearson and H.H. Lipowsky, Influence of erythrocyte aggregation on leukocyte margination in postcapillary venules of rat mesentery, *Am. J. Physiol. Heart Circ. Physiol*. **279** (2000), H1460–H1471.
[19] A.S. Popel and P.C. Johnson, Microcirculation and hemorheology, *Annu. Rev. Fluid Mech*. **37** (2005), 43–69.
[20] G. Segré and A. Silberberg, Behaviour of macroscopic rigid spheres in Poiseuille flow. II. Experimental results and interpretation, *J. Fluid Mech*. **14** (1962), 136–157.
[21] S.S. Shevkoplyas, T. Yoshida, L.L. Munn and M.W. Bitensky, Biomimetic autoseparation of leukocytes from whole blood in a microfluidic device, *Anal. Chem.* **77** (2005), 933–937.
[22] G.J. Tangelder, H.C. Teirlinck, D.W. Slaaf and R.S. Reneman, Distribution of blood platelets flowing in arterioles, *Am. J. Physiol. Heart Circ. Physiol*. **248** (1985), H318–H323.
[23] A.W. Tilles and E.C. Eckstein, The near-wall excess of platelet-sized particles in blood flow: Its dependence on hematocrit and wall shear rate, *Microvasc. Res*. **33** (1987), 211–223.
[24] G. Tryggvason, R. Scardoveli and S. Zaleski, *Direct Numerical Simulations of Gas-Liquid Multiphase Flows*, Cambridge Univ. Press, New York, 2011.
[25] B. Woldhuis, G.J. Tangelder, D.W. Slaaf and R.S. Renemann, Concentration profile of blood platelets differs in arterioles and venules, *Am. J. Physiol. Heart Circ. Physiol*. **262** (1992), H1217–H1223.
[26] C. Yeh and E.C. Eckstein, Transient lateral transport of platelet-sized particles in flowing blood, *Biophys. J*. **66** (1994), 1706–1716.
[27] J. Zhang, P.C. Johnson and A.S. Popel, in: *Computational Hydrodynamics of Capsules and Biological Cells*, C. Pozrikidis, ed., CRC Press, Boca Raton, FL, 2010.
[28] H. Zhao, E.S.G. Shaqfeh and V. Narsimhan, Shear-induced particle migration and margination in a cellular suspension, *Phys. Fluids* **24** (2012), 011902.
[29] H. Zhou and C. Pozrikidis, The flow of suspensions in channels: Single files of drops, *Phys. Fluids A* **5** (1993), 311–324.
[30] A. Zinchenko, M. Rother and R. Davis, A novel boundary-integral algorithm for viscous interaction of deformable drops, *Phys. Fluids* **9** (1997), 1493–1511.